Indian Journal of Pure & Applied Physics
Vol. 64, August 2026, pp. 880-889
DOI: 10.56042/ijpap.v64i8.31000

X-Ray Diffraction Based Structural Optimization and Electrical Properties of Nd^{3+} Doped $BaBi_2Nb_2O_9$ Aurivillius Ceramics

Mahima Momaliya[a], Helna Benny[a], Surya Pratap Singh[a], Manoj Verma[b] & Renuka Bokolia[a*]

[a]Department of Applied Physics, Delhi Technological University, Delhi 110 042, India

[b]Department of Physics, Hindu College, University of Delhi, Delhi 110 007, India

Received: 20th April 2026; accepted: 25th June 2026

Nd^{3+} doped $BaBi_2Nb_2O_9$ (BBN) ceramics were synthesized using conventional solid-state reaction route with optimized calcination (950 °C) and sintering (1050 °C) conditions to achieve phase purity. X-ray diffraction confirmed conformation of single-phase aurivillius framework with Fmmm space group. while scanning electron microscopy revealed a dense microstructure with a reduced, uniformly distributed grain size after Nd incorporation. FTIR analysis verified the presence of characteristic NbO_6 bonding, confirming structural stability. Ferroelectric studies showed well defined PE loops with decrease in maximum polarisation (P_m) from 12.85 μC/cm² to 8.47 μC/cm² upon Nd doping. Dielectric measurements showed a slight increase in dielectric constant (ε') from 255.77 to 267.30 at 455 K on Nd^{3+} doping along with reduced dielectric loss (ε") and stable frequency dependent behaviour. These properties confirm that Nd doped BBN is a potential alternative for lead free energy storage and capacitor applications.

Keywords: Energy storage ceramics, Rare-earth doping, Microstructure, Electrical properties, Dielectric relaxation

1 Introduction

Ferroelectric ceramics belong to a group of materials that show spontaneous electric polarization which can be reversed by applying an external electric field[1]. This behaviour arises due to the orientation of electric dipoles within small regions called domains. Because of this reversible polarization these materials are widely utilized in electronic devices such as sensors, actuators, capacitors, and nonvolatile memory devices[2]. Their ability to respond quickly to external electric fields and maintain stable polarization makes them highly useful for modern technology applications.

Apart from their ferroelectric property, materials such as $BaTiO_3$, $Pb(Zr,Ti)O_3$ (PZT), $LiNbO_3$, and $SrBi_2Ta_2O_9$ also exhibit excellent dielectric, piezoelectric, and optical properties, which make them useful for applications in capacitors, sensors, actuators, electro-optic devices, and non-volatile memory devices[3]. But the performance of the material depends significantly on its structure and chemical composition. Consequently, the method of modifying their properties by doping is gaining importance as an area of study.

Rare earth metals are a collection of metallic elements that comprise primarily the lanthanide series together with scandium and yttrium elements. They usually have trivalent oxidation states (RE^{3+}) and share identical chemical properties as a result of their nearly equivalent ionic radii[4]. As a consequence of these similarities, they can easily integrate within crystal lattices without creating significant structural distortions. The rare earth elements are widely used as dopants in ferroelectric materials such as barium titanate ($BaTiO_3$), lead zirconium titanate ($Pb(Zr,Ti)O_3$ or PZT), bismuth ferrite ($BiFeO_3$) and Aurivillius-type compounds like strontium bismuth niobate ($SrBi_2Nb_2O_9$), in which they significantly alter the structural, dielectric and ferroelectric characteristics of the host compound[5-7]. Research reports have revealed that rare earth dopants could enhance dielectric stability, lower leakage current, improve polarization properties and inhibit defect formation through effective control of oxygen vacancies and lattice distortion[7,8]. In addition, in layered ferroelectric systems, rare earth ions affect grain growth and microstructural homogeneity.

In recent times, there's been an increasing engrossment in developing lead free BLSF materials due to environmental and health protocols allied with lead-based compounds. As a result, researchers are focusing on alternative materials systems that are nontoxic and environmentally friendly. Among these

*Corresponding author: E-mail: renukabokolia@dtu.ac.in

Aurivillius type compounds also known as bismuth layered structured ferroelectrics (BLSFs) have attracted significant attention[9-11]. These materials have a unique layered structure consisting of alternating $(Bi_2O_2)^{2+}$ layers and perovskite blocks which gives rise to their characteristic anisotropic properties.

The general formula of an Aurivillius compound is $(Bi_2O_2)^{2+}$ $(A_{n-1}B_{n-}O_{3n+1})^{2-}$ where A site cations are generally larger than B site transition metals ions. The number of perovskite layers is represented by n which plays a prominent role in characterizing the material's behavior. Among these materials, barium bismuth niobate ($BaBi_2Nb_2O_9$ or BBN) is an important member with n=2 implying it contains two perovskite layers between the bismuth oxide sheets[8].

The relaxor behavior of the BBN material makes it ideal for energy storage, capacitors, and high-temperature applications because of the high maximum polarization and lower remnant polarization[1, 12]. Furthermore, BBN falls under the category of BLSF and has been proven to be a potential alternative to lead free ferroelectric materials and it is mainly because of its stability and resistance to fatigue[3, 9].

Among various dopants Neodymium (Nd^{3+}) is of particular interest in this paper because of its suitable ionic size and stable valence state. The ionic size of Nd^{3+} is comparable to that of Bi^{3+} which allows it to substitute easily into the lattice without causing significant structural distortion. This substitution can help improve lattice stability and minimize defect formation particularly oxygen related defects because of which better dielectric and ferroelectric properties can be achieved[5,13].

Previous studies on Nd doped Aurivillius compounds such as $SrBi_2Nb_2O_9$ have shown improvements in polarization behavior, dielectric stability, and fatigue resistance. These improvements have been associated with reduced defect concentration, suppression of oxygen-vacancy-related charge carriers, and improved structural stability induced by Nd^{3+} substitution at the Bi^{3+} site[14]. The reduction in defect-related conduction can contribute to enhanced polarization response, improved dielectric stability, and better fatigue endurance in Nd-doped systems. Therefore, it is expected that similar enhancements can be observed in Nd doped BBN systems as well.

In this work, Nd^{3+} is introduced into the BBN matrix to study its effect on structural, microstructural and ferroelectric properties. The analysis is carried out using unique techniques such as XRD, SEM, FTIR, polarization-electric field (PE loop) measurements and Dielectric measurements. The goal of this study is to attain the single phase formation of BBN and understand how Nd doping influences the material behavior and to evaluate its suitability for energy storage and ferroelectric applications[2,5].

2 Methodology

Undoped $BaBi_2Nb_2O_9$ (BBN) and Nd-doped $BaBi_{2-x}Nd_xNb_2O_9$ (where x= 0 and 0.10, corresponding to BN0 and BN1) were synthesized by solid state route by utilizing barium carbonate ($BaCO_3$, 99.9 %), bismuth(III) oxide (Bi_2O_3, 99.975 %), neodymium(III) oxide (Nd_2O_3, 99.99 %), and niobium(V) oxide (Nb_2O_5, 99.99 %) as starting precursor materials, all obtained from Sigma-Aldrich.

The starting materials were stoichiometrically mixed and subjected to wet milling using ethanol as the milling medium in a mortar and pestle for about 5 hours to allow for thorough mixing. Because of the volatility of bismuth at higher temperatures and therefore for achieving phase purity, an extra 2 wt % Bi_2O_3 was added to each sample, followed by further milling for 2 hours and drying. The resulting products were then heat-treated at 950 °C for 5 hours within alumina crucible. Following the calcination process, the samples were ground in a dry mill to eliminate any agglomeration and PVA used as a binding agent. The processed material was pressed uniaxially into 10 mm diameter pellets using hydraulic press and then sintered at 1050 °C for 3 hrs and the temperature was increased at a controlled rate of 2 °C/min. In heating cycle, there is a dwelling period of 1 hour at 600 °C to facilitate the burn-out of the binder. After sintering, both faces of each pellet were coated with silver paste to act as electrodes for electrical characterization.

A crystallographic structural analysis of the undoped and Nd doped $BaBi_2Nb_2O_9$ ceramics was conducted utilizing a Bruker D8 Discover high resolution XRD with Cu-Kα radiation (λ = 0.15406 nm). Surface morphology and microstructural characteristics were assessed using a JEOL JSM-6610LV scanning electron microscope (SEM), and the SEM images were analyzed through ImageJ software to calculate the average particle size. Dielectric measurements were performed utilizing a calibrated Keysight E4990 impedance analyzer within the defined frequency range (1 kHz-1 MHz). The

ferroelectric characteristics were assessed by capturing P-E hysteresis loops through Marine India advanced ferroelectric testing kit at 50 Hz frequency, with external electric field varying from 60 to 85 kV. (FTIR) analysis was carried out using a Perkin Elmer Spectrum-II spectrometer to identify functional groups and confirm the phase formation of the synthesized ceramics.

3 Results and Discussion

3.1 XRD

3.1.1 Optimization of Calcination Temperature

To establish the optimum conditions of calcination in the preparation of phase-pure $BaBi_2Nb_2O_9$ ceramics, a study was performed by varying parameters such as calcination temperature, heating duration, heating rate, and precursor composition. In the first step, the calcination temperature was varied between 850 °C to 950 °C at heating rate of 5 °C/min for 3 hours. XRD patterns of these samples were compared with the standard JCPDS card no. 00-012-0403, as shown in Fig. 1 (a). All samples exhibit the characteristic peaks of the aurivillius layered perovskite structure[10], with a progressive improvement in peak sharpness and intensity as the calcination temperature increases.

However, an additional impurity peak is observed in all cases, indicating incomplete phase formation. Among these, 950 °C was identified as the most suitable base calcination temperature, as it provides improved crystallinity while remaining below the threshold of excessive Bi_2O_3 volatilization. To further optimize the calcination conditions at 950 °C, the calcination duration and heating rate were varied. Although a noticeable improvement in peak sharpness was observed, the impurity peaks persisted, suggesting that the issue is not governed by heating kinetics but is primarily associated with Bi deficiency arising from Bi_2O_3 volatilization during calcination[15].

To compensate for the loss of Bismuth, 2 wt % excess Bi_2O_3 was introduced into the precursor composition, based on previous reports indicating that this level is optimal for achieving phase pure ceramics[16]. A lower addition may be insufficient to compensate for Bi loss, whereas a higher excess can lead to Bi_2O_3 segregation at grain boundaries, which is known to adversely affect the structural and electrical properties of the material[16].

The XRD pattern of the sample calcined at 950 °C for 5 hours with heating rate of 2 °C/min and 2 wt % excess Bi_2O_3 (Fig. 1 (b)) illustrates complete disappearance of impurity peak, confirming formation of single-phase Aurivillius layered perovskite structure. Therefore, these conditions were identified as optimal and were used for the preparation of all subsequent samples.

3.1.2 Optimization of Sintering Temperature

In order to ascertain the optimum sintering temperature for BBN ceramics, green pellets of the pure composition were sintered at 1000 °C, 1050 °C, and 1100 °C. Heating rate during the process was kept

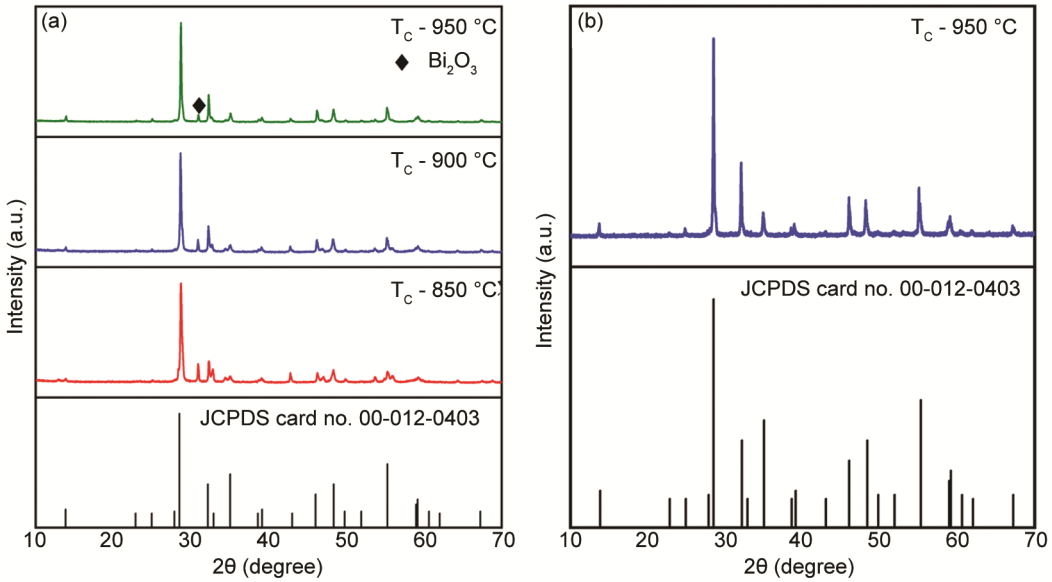

Fig. 1 — XRD patterns of $BaBi_2Nb_2O_9$ ceramics showing (a) temperature optimization for calcination; and (b) elimination of impurity phase upon addition of 2 wt % excess Bi_2O_3 at 950 °C

uniform at 2 °C/min for 3 hours. A pre-sintering treatment at 600 °C for 1 hour was also carried out prior to sintering to ensure the complete removal of the PVA binder used in pellet preparation[17]. This step is essential to prevent the incorporation of PVA residue into the sintered ceramic, which could otherwise compromise its structural and electrical properties.

XRD analysis of all three sintered samples, compared with JCPDS card no. 00-012-0403, is shown in Fig. 2. The patterns indicate that the Aurivillius phase is the dominant phase in all samples. However, the pellet sintered at 1000 °C, although confirming the Aurivillius perovskite structure, shows an apparent right shift in the diffraction peaks, indicating lattice contraction. This shift can be attributed to partial volatilization of Bi^{3+} ions during sintering, leading to A-site deficiency and consequent lattice distortion[15,18].

The pellet sintered at 1050 °C exhibits clear and sharp diffraction peaks, well matching the reference JCPDS data, suggesting high crystallinity, improved densification, and good lattice stability. In contrast, the pellet sintered at 1100 °C shows additional impurity peaks along with the primary Aurivillius phase peaks, indicating the formation of secondary phases, likely due to excessive bismuth loss at higher temperatures.

Thus, the optimal sintering temperature for BBN ceramic samples is determined to be 1050 °C[18], and these conditions were employed for the fabrication of all pure and Nd-doped BBN ceramic pellets.

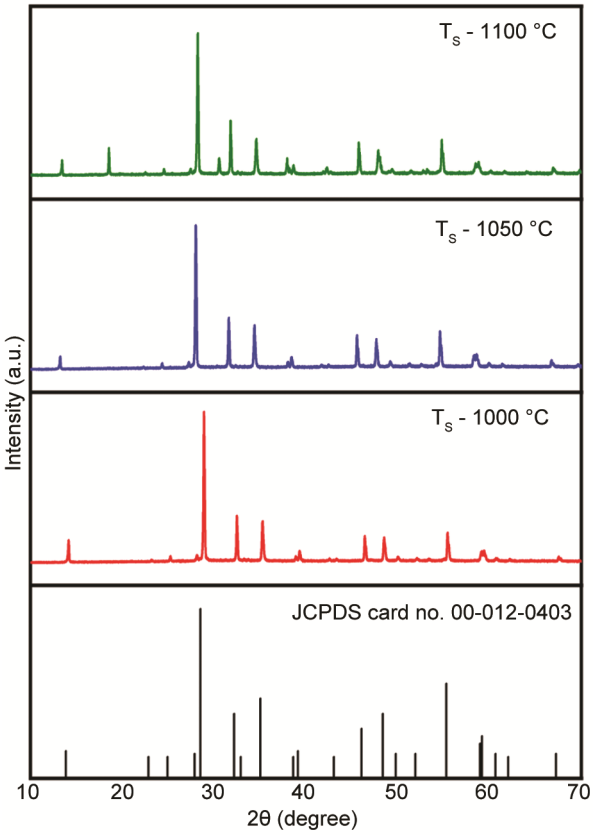

Fig. 2 — XRD spectra of $BaBi_2Nb_2O_9$ ceramics sintered at 1000°C, 1050°C and 1100°C, compared with the standard JCPDS card no. 00-012-0403, showing the effect of sintering temperature on phase purity

3.1.3 Phase Analysis of Pure and Nd Doped BBN Ceramics

X-ray diffraction (XRD) patterns of pure (BN0) and Nd-doped (BN1, x = 0.1) $BaBi_2Nb_2O_9$ (BBN) ceramics are presented in Fig. 3, together with the standard reference pattern (JCPDS card no. 00-012-0403)[13]. All the peaks in XRD patterns of the pure and Nd-doped BBN ceramics correspond well with the standard pattern. Thus, the pure as well as the Nd-doped BBN ceramics have a uniform Aurivillius layered perovskite structure characterized by orthorhombic symmetry.

The intense peak at the (115) plane reveals the characteristic layered structure of BBN (m = 2)[18-19]. The absence of impurity peaks suggests successful incorporation of Nd ions into lattice. It's also observed from the figure that the diffraction peaks of the Nd-doped BBN ceramics are shifted towards the lower angles compared to the pure BBN ceramics.

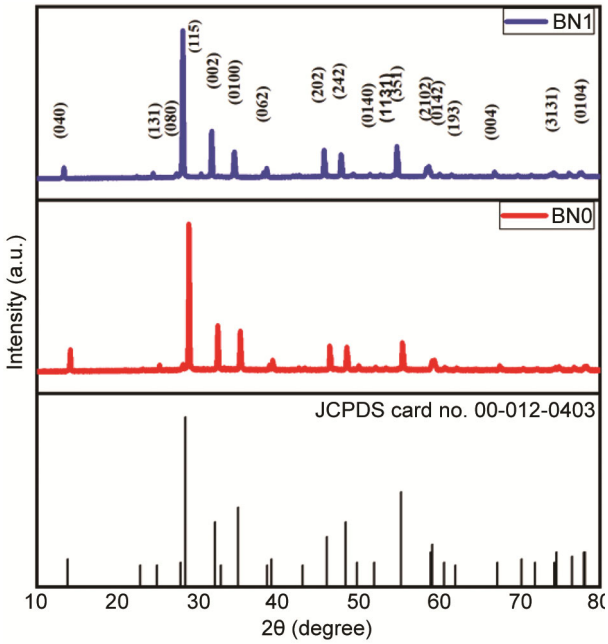

Fig. 3 — XRD spectra of pure (BN0) and Nd-substituted (BN1) $BaBi_2Nb_2O_9$, compared with the standard JCPDS card no. 00-012-0403

Such shifts towards lower diffraction angles indicate an increase in the interplanar-spacing according to Bragg's law, which is consistent with an expansion of the unit cell volume. This expansion is reflected in the increase of the orthorhombic lattice parameters (a, b, and c), and may be attributed to the substitution of Nd^{3+} ions at Bi^{3+} sites, leading to lattice distortions due to the difference in ionic radii[17].

Although the ionic radius of Nd^{3+} is close to the Bi^{3+} ions the observed lattice modifications may because of the stereochemical activity of $6s^2$ lone pair electrons of Bi^{3+}, which influence the local coordination environment. The lattice modifications, which have occurred after the doping of Nd^{3+} ions, are related to the replacement of the Bi^{3+} ions, which have the stereo chemically active lone pair electrons. The lattice parameters have expanded, as the Nd^{3+} ions have replaced the Bi^{3+} ions[20-21].

3.2 SEM

The topography of processed samples was studied using SEM and images are attached in Fig. 4 and the grain-size distribution histogram is depicted in Fig. 5. Both the undoped (BN0) and Nd doped (BN1) samples show compact microstructure with well-developed grains indicating the sintering process was

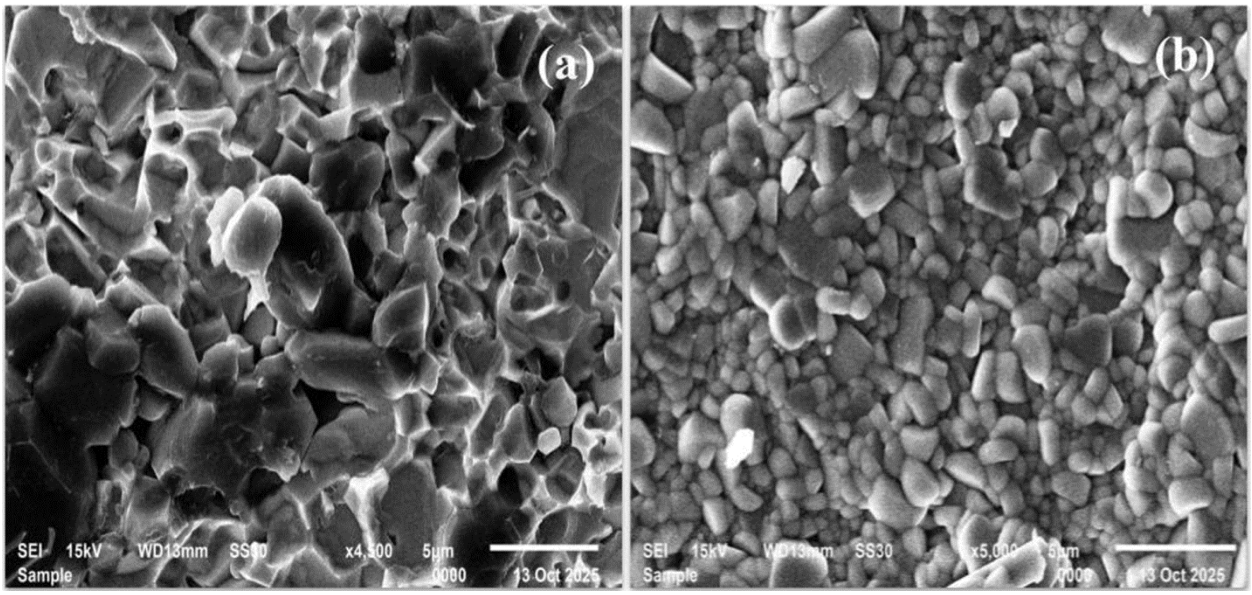

Fig. 4 — SEM microstructures of (a) pure $BaBi_2Nb_2O_9$ (BN0); and (b) Nd^{3+} substituted $BaBi_2Nb_2O_9$ (BN1)

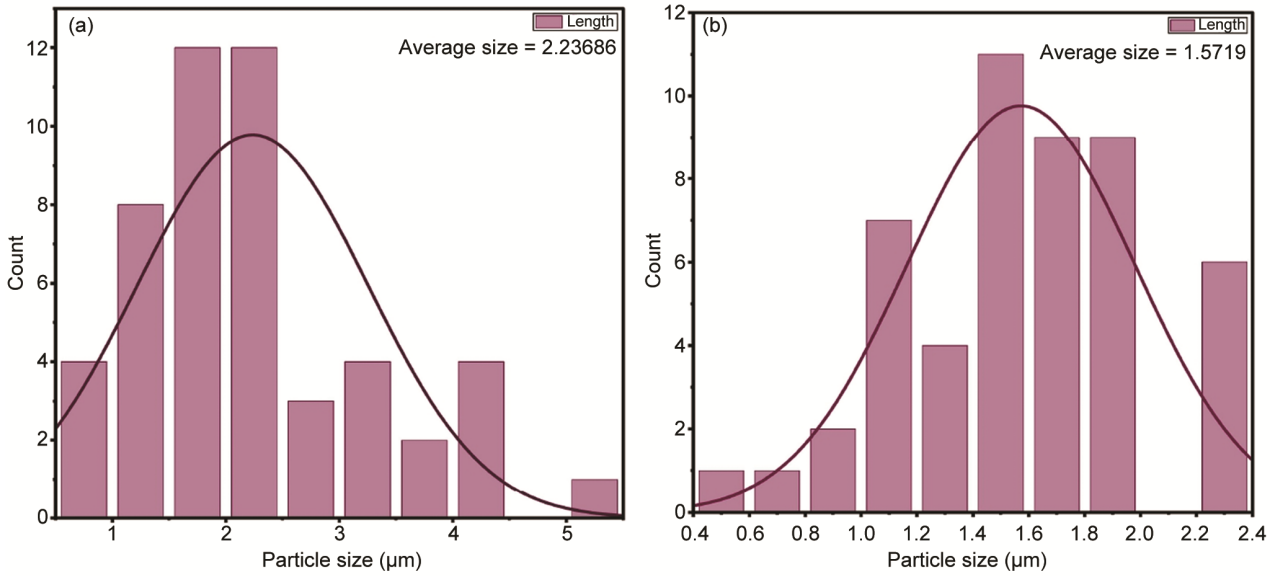

Fig. 5 — Histogram distribution of grain size for (a) BN0; and (b) BN1 samples obtained from SEM micrographs using imageJ analysis

effective. No major pores and cracks are observed which suggests good compactness of the material.

The grains in both compositions exhibit a plate-like shape which is a common feature of aurivillius-type layered ferroelectric materials[9]. A noticeable change is observed after Nd addition. The undoped sample contains relatively larger grains whereas the Nd doped sample shows lesser but more uniformly distributed grains.

Average grain size was calculated using ImageJ software, and a reduction in grain size is noted in the sample BN1. This phenomenon can be explained by the substitution of Bi ions with Nd ions which influences grain growth during sintering. The presence of Nd slows down grain boundary movement resulting in restricted grain growth and finer microstructure. The reduction in grain growth after doping with Nd is due to the presence of Nd^{3+} ions in the grain boundaries, making their movement difficult during sintering. The difference in size of the Nd^{3+} and Bi^{3+} ionic radii causes lattice stress and defects, restricting the motion of the ions and hindering grain boundary migration, thereby resulting in restricted coalescence of the grains[22]. Similar trends have been reported in other rare earth modified layered ferroelectric systems[23]

The plate-like structure can be related to anisotropic crystal growth, where growth along certain crystallographic directions is more favorable than others leading to layered grain formation[24]. Overall the Nd doped (BN1) sample shows a more refined and uniform microstructure compared to the undoped sample (BN0).

3.3 Analysis of Fourier Transform Infrared (FTIR)

The FTIR spectra of BN0 and Nd doped BN1 sample exhibit prominent absorption bands around 566 cm^{-1}, 618 cm^{-1} and 822 cm^{-1} which is assigned to the bending and stretching vibrations of Nb—O bonds within the NbO_6 octahedral units shown in Fig. 6[4,7,21]. A noticeable shift in bending vibration from 618 cm^{-1} (BN0) to 624 cm^{-1} (BN1) is observed after Nd^{3+} incorporation shown in Figs. 7 and 8. This shift towards higher wavenumber suggests a modification in the local bonding environment indicating that Nd ions are effectively incorporated into the lattice[7].

The full width at half maximum values (FWHM) for both compositions remains nearly unchanged, as listed in Table 1 implying that the introduction of Nd does not significantly disturb the structural order or induce notable lattice disorder. The absence of peak broadening suggests that the NbO_6 octahedral framework is largely preserved[12].

The shift in the FTIR peak can be explained by changes in the strength of Nb—O bond caused by introduction of Nd ions into the structure. This shows

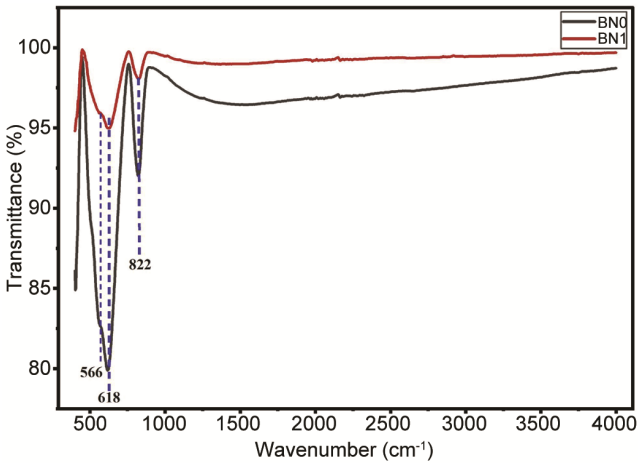

Fig. 6 — Fourier transform infrared (FTIR) data obtained at room temperature for BN0 and BN1 with prominent absorption peaks marked on 566 cm^{-1}, 618 cm^{-1} and 822 cm^{-1}

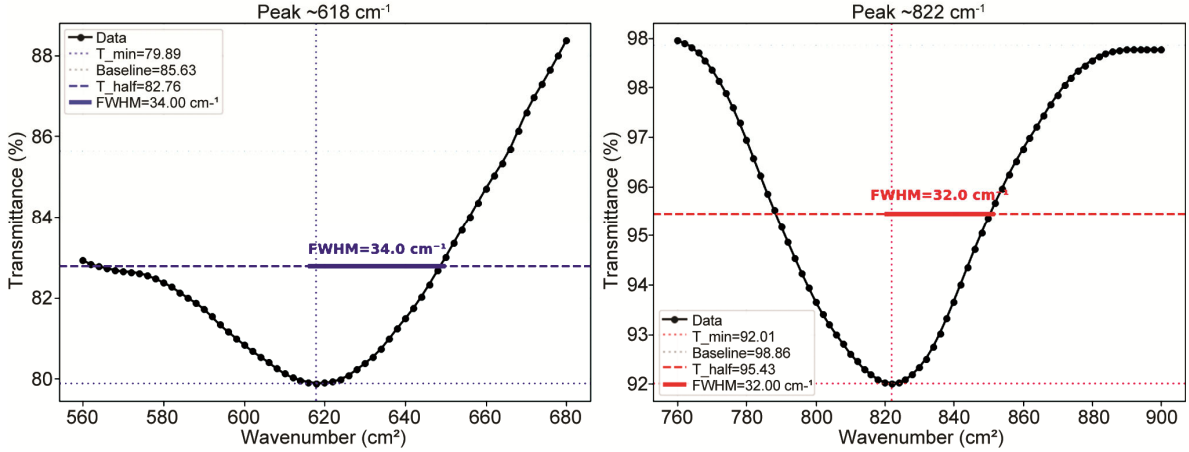

Fig. 7 — FWHM analysis of FTIR absorption bands of BN0 at 618 cm^{-1} and 822 cm^{-1} using Direct method

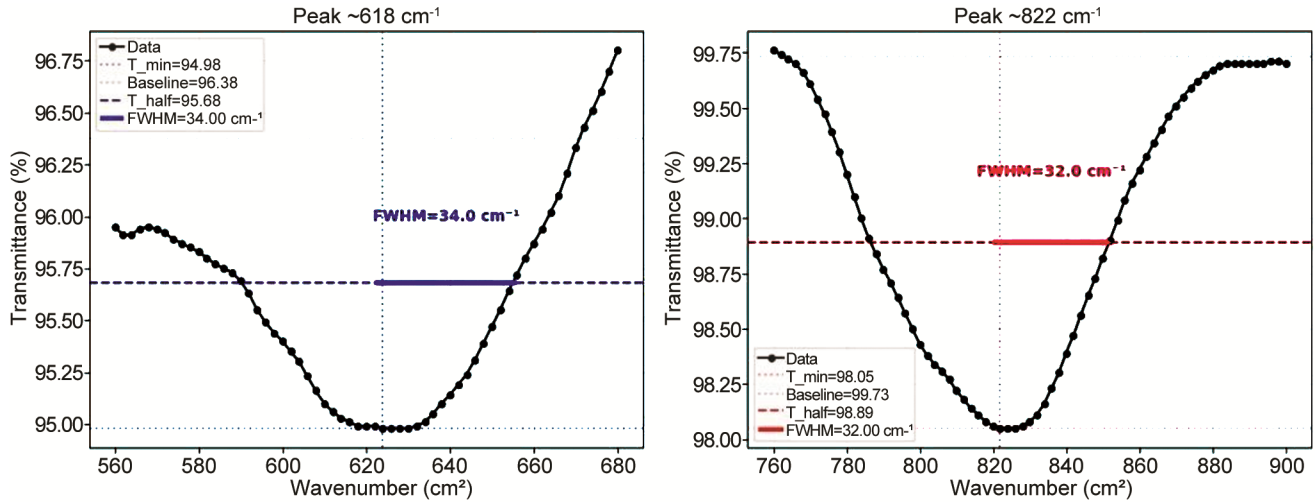

Fig. 8 — FWHM analysis of FTIR absorption bands of BN1 at 624 cm^{-1} and 822 cm^{-1} using Direct method

Table 1 — Vibrational modes, corresponding wavenumbers, and FWHM values of FTIR absorption bands for BN0 and BN1

Sample	Vibrational Mode	Wavenumber (cm^{-1})	FWHM (cm^{-1})
BN0	Nb–O bending	618.00	34.00
BN0	Nb–O stretching	822.00	32.00
BN1	Nb–O bending	624.00	34.00
BN1	Nb–O stretching	822.00	32.00

that doping affects the local bonding environment but the overall crystal structure remains stable. This observation is also supported by the XRD results[9, 25].

3.4 Analysis of P-E Hysteresis Loop

The polarization electric field loops of BBN (BN0) and Nd activated BBN (BN1) were recorded at 27 °C to evaluate their ferroelectric characteristics. Both the compositions exhibit closed and well defined hysteresis loops confirming the presence of ferroelectric ordering[26, 27].

The pure sample shows a relatively broader loop with higher maximum polarization (P_m) and remnant polarization (P_r) which can be observed in Fig. 9 (a)-(b). In contrast, the Nd doped sample composition exhibits a comparatively slimmer loop with reduction in polarization values. The maximum polarization (P_m) decreases from 12.85 μC/cm² (BN0) to 8.47 μC/cm² (BN1) and remnant polarization ($2P_r$) decreases from 3.69 μC/cm² to 1.82 μC/cm² after Nd addition. This behavior shows that Nd addition changes the domain behavior and reduces the long-range ferroelectric ordering, indicating a shift towards relaxor like characteristics[1,28].

The observed decrease in polarization can be credited to defects formed particularly by the formation of oxygen vacancies during high-temperature processing. In bismuth layered structure ferroelectrics, volatilization of Bi^{3+} often leads to lattice defects, which act as pinning centres and hinder domain wall motion[8]. Additionally, microstructural refinement due to reduced grain size further restricts polarization switching, contributing to the observed loop slimming[12].

The PE loops were further investigated to determine the energy storage parameters which include total energy density and recoverable energy density using standard relations mentioned below.

$$W = \int_0^{p_m} EdP$$

$$W_{rec} = \int_{P_r}^{P_m} EdP$$

where P_m is maximum polarization and P_r is remnant polarization[28].

The values of remnant polarization (2Pr), maximum polarization (Pm), total energy density (W), recoverable energy density (Wrec) and coercive field obtained from P–E hysteresis loops are listed in the Table 2. The slimmer loop observed for the Nd doped composition indicates reduced hysteresis loss and improved energy storage efficiency, which is desirable for dielectric capacitor applications[29].

3.5 Dielectric Behaviour Analysis

The variation of dielectric constant (ε') with temperature for pure (BN0) and Nd-doped (BN1) $BaBi_2Nb_2O_9$ samples at varying frequencies is illustrated in Fig. 10 (a)-(b).

Dielectric constant increases with increase in temperature, indicating ferroelectric-paraelectric

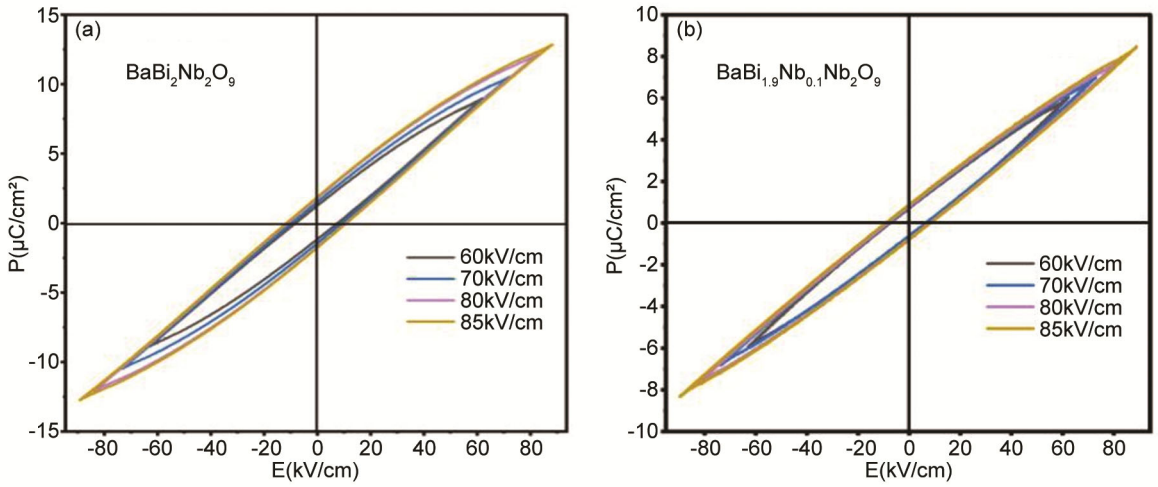

Fig. 9 — P–E hysteresis loops of (a) BN0; and (b) BN1 compositions recorded at different applied electric fields

Table 2 — Values of remnant polarization (2Pr), maximum polarization (Pm), total energy density (W), recoverable energy density (Wrec) and coercive field obtained from P–E hysteresis loops for BN0 and BN1 ceramics

PARAMETERS	COMPOSITIONS	
	BN0	BN1
$2P_r(\mu C/cm^2)$	3.68564	1.81698
$P_m(\mu C/cm^2)$	12.85574	8.47099
$W(J/cm^3)$	0.60576	0.41333
$W_{rec}(J/cm^3)$	0.42964	0.31732
Coercive field (kV/cm)	11.1900	8.5376

transition. Dielectric constant decreases with increasing frequency because of limited response of dipolar polarization.

For the pure sample (BN0), the maximum dielectric constant (ε'_m) is found to be 255.7 at transition temperature of 454 K. In contrast, the dielectric constant of the Nd-doped (BN1) sample is found to be slightly higher, with a value of 267.3. In both cases, the transition temperature is nearly the same, with a value of 455 K[30].

The broadening of the dielectric peak for the doped material can be attributed to increased lattice disorder. This may be attributed to the Nd^{3+} ion doping, which causes local lattice distortions affecting the ferroelectric transition[31].

Frequency dependence of dielectric constant (ε') of pure BN0 and Nd-doped BN1 $BaBi_2Nb_2O_9$ ceramics at room temperature is presented in Fig. 10 (c). It was observed that dielectric constant of both ceramics decreases with increasing frequency due to the limited polarizability of the dipoles at higher frequencies. At lower frequencies, dipoles are able to align with applied field, thereby contributing significantly to the polarization; however, at higher frequencies, they fail to follow rapidly changing field, resulting in a decrease in the dielectric constant. This kind of behavior in the dielectric constant is generally termed dielectric dispersion[32]. The Nd-doped ceramic (BN1) has a higher value of dielectric constant when compared with the pure ceramic (BN0) for all the measured frequencies, which agrees well with the temperature-dependent dielectric data. Dispersion is much more pronounced at low frequencies, and with an increase in the frequency, the difference in dielectric constants between the two ceramics gradually decreases, reaching almost the same values at high frequencies[33].

The temperature dependence of the dielectric loss (ε'') for BN0 and BN1 samples at varying frequencies is illustrated in Fig. 11. Dielectric losses for both samples remain small and almost stable at lower temperatures, meaning that there is a minimum dissipation of energy. With the increase of the temperature, the dielectric loss also increases gradually with a sharp increment at high temperatures especially at lower frequencies, which may be related to the effect of charge carriers and space charges[33-34]. A slight peak in the middle temperature regime (400–500 K) is detected for both samples, which is probably because of the phase transition between ferroelectricity and paraelectricity, as explained by the dielectric constant measurement.

The dielectric loss shows clear dispersion behavior, being significantly higher at lower frequencies compared to higher frequencies. This is because at lower frequencies, charge carriers have sufficient time

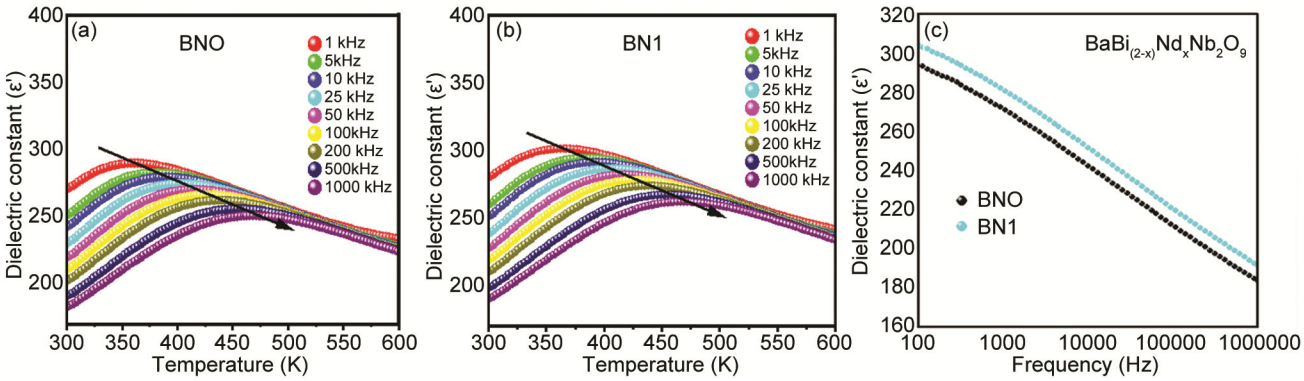

Fig. 10 — Temperature dependence of the dielectric constant (ε') at varying frequencies (1 kHz - 1000 kHz) for (a) BN0, (b) BN1; and (c) frequency dependence of ε' for BN0 and BN1

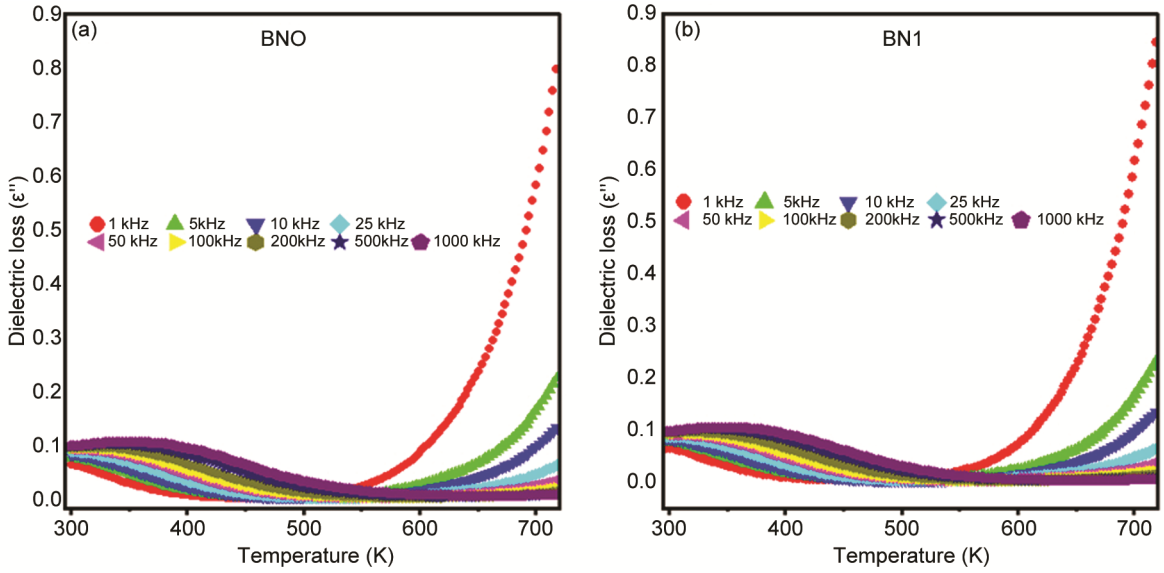

Fig. 11 — Temperature dependence of the dielectric loss (ε'') at varying frequencies (1 kHz – 1000 kHz) for (a) BN0; and (b) BN1

to respond to the applied field, contributing more to energy dissipation, whereas at higher frequencies the dipoles are unable to follow the rapidly alternating field, resulting in reduced dielectric loss[35]. In comparison with BN0 the BN1 samples exhibit lower dielectric loss, suggesting that Nd^{3+} doping suppresses mobility of charge carriers, therefore reducing energy dissipation.

The decrease in dielectric constant with increasing frequency indicates non-Debye type relaxation behavior in the ceramics. This behavior can be explained using Maxwell–Wagner interfacial polarization and Koop's theory, where the material consists of conducting grains separated by highly resistive grain boundaries. At low frequencies, charge carriers get accumulated at the grain boundaries and contribute more to polarization, resulting in higher dielectric constant values. However, at higher frequencies, the dipoles and charge carriers are unable to follow the rapidly changing electric field, causing the dielectric constant to decrease[32-37].

Dielectric measurements show that doping with Nd causes a slight improvement in the dielectric properties, retaining thermal stability. This can be associated with the structural changes observed during the XRD analysis.

4 Conclusion

In this work, pure and Nd doped $BaBi_2Nb_2O_9$ (BBN) ceramics were successfully synthesized with help of conventional solid state route, with optimized calcination and sintering temperature, ensuring phase purity and good crystallinity. X-ray diffraction analysis confirmed the formation of single phase

Aurivillius layer structure for both compositions while the observed peak shifts after Nd incorporation indicate slight lattice modifications. Microstructural analysis revealed dense and well developed plate like grains in both samples, which is a characteristic of layered ferroelectrics. Reduction in the average grain size was observed in the Nd doped composition suggesting that Nd incorporation effectively suppresses grain growth and leads to more uniform microstructure.

Ferroelectric measurements demonstrated well defined PE hysteresis loops confirming the ferroelectric nature of the materials. The Nd doped sample exhibits reduced maximum (P_m) and remnant polarization ($2P_r$) values, indicating a transition towards relaxor behavior. On the other hand, a slimmer hysteresis curve implies lesser energy loss and therefore high efficiency when it comes to storing energy. From the investigations on dielectric behavior, both types of compounds have similar transition temperature although in case of Nd doped compound there is some improvement in the value of dielectric constant (ε') and reduction in dielectric loss (ε'') and better stability at higher frequencies. This might have been caused by defects introduced in the structure due to Nd doping.

Overall, it can be concluded that doping with Nd3+ ion significantly affects the characteristics of BBN ceramic material. The superior dielectric and low hysteresis loss characteristics make it a suitable candidate for lead-free ferroelectric applications.

References

1 Cross L E, *Ferroelectrics*, 76 (1) (1987) 241.
2 Scott J F, *Sci*, 315 (5814) (2007) 954.
3 Cotton F A, Wilkinson G, Murillo C A & Bochmann M, *Advanced Inorganic Chemistry*, 6th edn (John Wiley & Sons, New York) 1999.
4 Haertling G H, *J Am Ceram Soc*, 82 (4) (1999) 797.
5 Priya S & Nahm S, *Lead-Free Piezoelectrics* (Springer, New York) 2012.
6 Aurivillius B, *Ark Kemi*, 1 (1949) 499.
7 Newnham R E, *Structure–Property Relations* (Springer, Berlin) 1975.
8 De Araujo C A-P, Cuchiaro J D, McMillan L D, Scott M C & Scott J F, *Nature*, 374 (6523) (1995) 627.
9 Benny H, Momaliya M, Singh S P *et al*., *Ceram Int*, 52 (18) (2026) 33731.
10 Shahni S, Bokolia R, Singh S P *et al*., *Ceram Int*, 51 (24A) (2025) 41251.
11 Sharma R *et al*., *Mater Adv*, 5 (21) (2024) 8638.
12 Han S-H, Cho S Y & Bu S D, *Curr Appl Phys*, 71 (2025) 9.
13 Al-Aaraji M N, Feteira A, Thompson S P, Murray C A & Hall D A, *J Eur Ceram Soc*, 39 (14) (2019) 4070.
14 Khare V, Garg D, Singh S P *et al*., *Appl Phys A*, 132 (71) (2026).
15 Shigyo T, Itoh H & Takahashi J, *J Mater Sci Mater Electron*, 21 (3) (2010) 302.
16 Basith A, Singh S, Banwal A, Narwan M, Verma M & Bokolia R, *Ceram Int*, 50 (24) (2024) 52344.
17 Zulhadjri, Rizki A, Wendari T P & Putri Y E, *Mater Chem Phys*, 331 (2025) 130177.
18 Shannon R D, *Acta Crystallogr Sect A*, 32 (5) (1976) 751.
19 Banwal A & Bokolia R, *J Lumin*, 263 (2023) 120071.
20 Banwal A, Verma M, Singh B & Bokolia R, *Appl Phys A*, 130 (5) (2024) 334.
21 Wulff G, *Z Kristallogr Cryst Mater*, 34 (1) (1901) 449.
22 Nakamoto K, *Infrared and Raman Spectra of Inorganic and Coordination Compounds: Part A: Theory and Applications in Inorganic Chemistry, 6th edn* (John Wiley & Sons, Hoboken, NJ) 2008.
23 Griffiths P R & de Haseth J A, *Fourier Transform Infrared Spectrometry* (Wiley-Interscience, New York), 1986.
24 Smolensky G, "Ferroelectrics with diffuse phase transition," *Ferroelectrics*, 53 (1) (1984) 129.
25 Lines M E & Glass A M, *Principles and Applications of Ferroelectrics and Related Materials*, (Clarendon Press, Oxford) 1977.
26 Jaffe B, Cook Jr W R & Jaffe H, *Piezoelectric Ceramics* (Academic Press, London) 1971.
27 Smolenskii G A & Agranovskaya A I, *J Tech Phys*, 28 (1958) https://www.osti.gov/biblio/4294595.
28 Zhang Q M, Wang H, Kim N and Cross L E, *J Appl Phys*, 75 (1) (1994) 454.
29 Ogihara H, Randall C A & Trolier-McKinstry S, *J Am Ceram Soc*, 92 (8) (2009) 1719.
30 Thakur S, Shandilya M, Graça M P F & Valente M A, *Ferroelectr Lett Sect*, 47 (4) 76.
31 Zheng Q, Luo L, Lam K H, Jiang N, Guo Y & Lin D, *J Appl Phys*, 116 (18) (2014) 184101.
32 Sharma A & Mehta N, *RSC Adv*, 7 (31) (2017) 19085.
33 Thakur S, Shandilya M, Graça M P F & Valente M A, *Ferroelectr Lett Sect*, 47 (4) (2020) 76.
34 Mahani R M & Omara S, *Appl Phys A*, 128 (8) (2022) 706.
35 Tayari F *et al*., *Ceramics*, 7 (3) (2024) 958.
36 Koops C G, *Phys Rev*, 83 (1951) 121.
37 Achard F, in *Landmark Writings in Western Mathematics*, (Elsevier, Amsterdam) 2005, p. 564.